IDENTIFICATION OF ELECTRONS AT THE SSC

G. Brandenburg	Harvard University
J. Butler	Fermilab
Y. Ducros	Saclay
Y. Fukui	Fermilab
P. Grannis	SUNY, Stony Brook
J. Linnemann	Michigan State University
D. Wagoner	Florida A & M University
A. Yamashita	Tsukuba University

1. Introduction

The importance of identifying electrons produced in very high energy hadron collisions has been stressed widely in discussions of the physics and detectors for the SSC.[1-4] The strategies for identifying electrons have been explored in these earlier Snowmass workshops and in specialized detector workshops. The effort during Snowmass 1986 was centered on refining the methods for electron measurements and on understanding the requirements to be imposed upon tracking detectors and calorimeters.

This report is divided into four main sections. In section 2, we summarize some of the requirements for electron identification which emerge from a consideration of the likely physics topics at the SCC. In section 3, new work on specific methods (calorimetry, transition radiation detection and synchrotron radiation detection) is discussed. Discussion of the backgrounds to be encountered in electron measurements is found in section 4; some considerations for overall detector design are presented in section 5.

2. Physics Requirements on Electron Identification

Electron identification will be an important aspect in recognizing many of the physics signatures of interest at the SSC.[5,6,7]. We summarize here only a few processes which are likely to give constraints on electron identification in various kinematic domains.

Among the topics which emphasize the need for electron identification at low p_T is $t\bar{t}$ production[8], for example by the decay of a techni-eta. An interesting $t\bar{t}$ mass range is .2 to 1 TeV, resulting in t jets with p_T = 0.1 to 0.5 TeV. Thus the scale of interesting lepton momenta is (for the 3-body decay $t \to b\ e\ \nu$ decay $p(e) \sim p(t)/3$, or 20 to 150 GeV/c. Within this range, the sort of analysis forseen requires a rejection factor of hadrons in favor of isolated leptons of 2-5 x 10^3.

The search for supersymmetric particles will also impose some requirements on electron identification[9]. Here the signal is missing p_T and the absence of leptons. One needs the electron (or muon or tau) identification to tag those events with heavy quarks produced, in which energetic neutrinos could simulate the missing p_T expected from gluinos, etc.. Because the lepton momentum is anticorrelated with the neutrino momentum, one would like lepton identification to be good at low energies. However, there is a limit on the ability to reject heavy quark backgrounds to SUSY processes imposed by the decays into taus with subsequent tau decay to ν + hadrons.

Another process which places emphasis on electron identification at low electron momentum is production of charged Higgs particles by $b\bar{t}$ fusion[6]. The presence of a spectator t quark in the beam jet is a useful tag after the main $H \to b\bar{t}$ decay into an isolated lepton has been seen. One requires the identification of electrons with $p_T \sim 10$ GeV/c ($p \sim 30$ GeV/c) in an eta range 1.5 to 4. Fortunately, the rejection required only of order 10^2, as other cuts can do most of the selection job.

One of the physics signatures which places the most stringent demands on identification of low momentum electrons is the study of b decays[3]. In the TASTER detector[10] for forward b quark detection (eta 2 to 5), one would search for leptons with $p \sim 20$-40 GeV. The problem of overlaps with other jet particles is addressed in this detector design by allowing a large drift space to separate the particles, so that the ability to recognize electrons in a high density environment of hadrons can be enhanced.

A process which stresses electron identification at very high electron energies is the production of a W' or Z'.[5] Here, the lepton has a typical p_T of order M/2. The discovery limit at the SSC is of order 7 TeV; the signal from a W' of 1 TeV mass is seen to be relatively clean if a hadron rejection of order 1000 can be obtained out to a limit of 500 GeV p_T; leptons should be well isolated from jets for this sort of process.

A more systematic compendium of requirements on electron identification as a function of energy, angle and isolation from other particles would be of considerable use. The qualitative conclusion reached during Snowmass 86 is that below 100 GeV/c, many physics signatures will benefit from hadron rejection power at the level of 10^5, whereas for the regime above 1 TeV/c, rejections at the level of 10^3 should suffice.

3. Electron Detection Methods

3.1 Calorimetry

Many previous studies have been performed which explore methods for distinguishing electrons and hadrons based upon the observed shower shape in a calorimeter. Several of these are summarized in Ref. 2. It has been

clearly established that high energy electrons can be distinguished from hadrons with rejection factors approaching 1000 : 1. The important considerations for design of the EM calorimeter include transverse and longitudinal segmentation and energy resolution, together with the external questions of whether magnetic analysis is available and the nature of a hadron calorimeter following the EM detector.

The general questions addressed in this workshop were (a) optimization of the calorimeter parameters for best electron identification and (b) improvements in the methodology of electron selection in order to find faster and more efficient algorithms appropriate to the large information density in SSC calorimeters.

The use of calorimeter information to study the rejection of hadrons as electron candidates was reported in a paper contributed to these proceedings[11] by Y. Fukui, et. al using test data from a CDF calorimeter study. The general method[12] is to calculate a generalized chi-square variable for an individual event to fit the hypothesis of being an electron. The method uses a full covariance matrix evaluated on electron test beam data, thus taking into account not only the average properties of the variables $[v_i]$ studied, but their correlations:

$$M_{ij} = \frac{1}{N} \sum_n (v_i^{(n)} - \bar{v}_i)\,(v_j^{(n)} - \bar{v}_j)$$

$$H = M^{-1}$$

$$\zeta_m = \sum_{i,j} (v_i^{(m)} - \bar{v}_i)\, H_{ij}\, (v_j^{(m)} - \bar{v}_j)$$

The parameter ζ_m is a chi-square measure of how well event m adheres to the mean values and correlations of $[v_i]$ appropriate to the calibration sample used to determine M.

This form is valid for any choice of variables. Practical application requires parameterization of the H matrix and the mean values $[\bar{v}_i]$ of the variables used, as a function of deposited energy in the calorimeter, incidence angle, and incidence position. In the original publication, the variables chosen were simply cell energy depositions, which make such parameterization difficult. The first contribution of Fukui et al was to recognize that using ratios of energy deposition in depth layers to total deposition in the electromagnetic calorimeter removes the first-order energy variation of the variables and thus of the covariance matrix and mean variable values. The important second contribution is the use of variables other than energy deposits. The specific analysis employed energy-weighted rms widths as a measure of transverse shower size which gives a size measure independent of the impact point.

The basic issues studied in this work are the relative importance of various longitudinal and transverse segmentations. In interpreting the results, it is well to recall that only a particular segmentation was studied, and only at a single energy (100 GeV). Conclusions about the optimal disposition of longitudinal segments should be made recalling that in the range of 25 to 500 GeV electron showers, the shower maximum moves back by about 3 radiations lengths. The eta and phi strips cover different areas than the pads, but the showers were contained within both the pads and the strips. The eta and phi strips are in fact interleaves[11] within part of the second electromagnetic segment, so that one would expect that there are effectively 5 independent depth measurements in the calorimeter:

EM1, eta + phi, EM2-(eta + phi), EM3, and HAD

which correspond to 2.5, 5, 7, and 2.5 radiation lengths, then 6 interaction lengths. Dropping the eta and phi deposition information corresponds to coarsening this to (2.5, 12, 2.5 r.l). The total EM thickness is only 17 X_o. The energy resolutions obtained in this calorimeter are relatively large (0.24 $\sqrt{E}$ and 1.32 $\sqrt{E}$ for EM and hadron sections respectively).

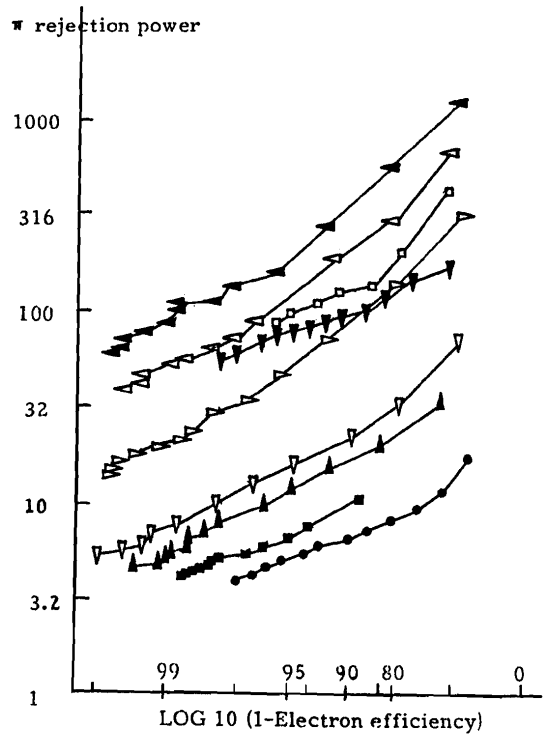

Fig. 1. π rejection power as a function of electron efficiency for 100 GeV e^- and π^- events. The set of variables used is denoted by:

- EM1,EM2,EM3/EM $+\eta+\phi$ $+\sigma_\eta+\sigma_\phi$ +HAD/EM
- EM1,EM2,EM3/EM $+\eta+\phi$ +HAD/EM
- EM3,(EM1+EM2)/EM
- EM1,EM2,EM3/EM $+\eta+\phi$ $+\sigma_\eta+\sigma_\phi$ HAD/EM
- EM1,EM2,EM3/EM $+\eta+\phi$
- EM1,EM2,EM3/EM
- EM3,(EM1+EM2)/EM
- EM1,(EM2+EM3)/EM

Figure 1 shows the pion rejection factor from the analysis in Ref. 1. First, one notes if one requires an electron efficiency about 90%, the ratio of deposit after 17 X_o to the deposit in the first 17 X_o gives a rejection of order 50, and that this rejection is comparable to the rejection obtained from full use of the longitudinal and transverse information, but ignoring the deposition after 17 X_o. The additonal rejection obtained by using segmentation internal to the EM calorimeter in addition to the hadronic deposition is a factor of 2 to 5. The rejection beyond this (for the same net electron efficiency) obtained by using the transverse shower size, is another factor of 2 to 3. The overall rejection factor of 400 for 100 GeV pions is

consistent with previous measurements[2]. Note that this analysis has not directly used the energy deposit in the EM section. The energy deposit enters only through ratios and one may enquire whether a more optimal set of variables can be found. As noted above, the advance made in this study has been in a more efficient choice of variables to be used in the correlation matrix method, enabling easier parametrization in the important detector variables.

Some progress was also made on more general questions of pion-electron discrimination in work performed by J. Linnemann. It is useful to compare the covariance method outlined above with the method of recursive binary partition[13,14]. In this method, one chooses a set of variables and builds a decision tree using them. One considers a set of "good" events (here electrons) and a set of "bad" events (here pions). At each stage of the decision, one chooses the variable and the cut value in that variable which best distinguishes the good and bad events. The next step is to consider the two subsamples thus obtained, and separately for each sub-sample, again choosing the best variable and best cut; the process continues step by step, hopefully ending with 2^n subsamples, each labelled as good or bad.

One strength of this procedure is that it automatically selects the most effective variables out of a set of candidate variables. Another strength is that there is a natural way of introducing information about both the "good" and the "bad" events. However, if two of the chosen variables are correlated, it does not always use that information effectively, but must always choose one or the other. Further, since the whole procedure is a tree of many steps, there is some difficulty in parameterizing the tree as a function of externally varying variables, for example incident energy or incidence angle. Finally, in the simplest formulation of the method, each cut is a single-sided cut, so that a two-sided cut (separating a peak from its tails) appears as two distinct steps.

In contrast, the correlation-matrix method automatically makes best linear combinations of variables (though it does rather worse than the recursive partition in dealing with non-linearly correlated variables). One might criticize its failure to offer automatic guidance in the choice of the most effective variables. One must calculate a new matrix and run through the data again with each choice of new set of parameters. In addition, there seems to be no useful way to introduce information about the "bad" sample. However the method is simple, relatively intuitive, and results in a single variable for discriminating e and hadron.

We offer here a rough method to address some of these concerns in the correlation matrix method. First, consider the question of reducing the number of parameters in the H matrix. The method of principal components[15] suggests a means of obtaining a more compact set of variables which convey the most important information about the electron showers. One simply diagonalizes the covariance matrix H. This gives a new set of variables which are linear combinations of the original ones chosen. These might be a better set of variables than the original set as an input to the recursive partion method, as the linear correlations among variables are removed by this procedure. In fact, this even gives an ordering criterion for dropping variables: namely the size of their variances.

The mere size of the variance is not really the chief criterion for the utility of a variable; it only represents how important the variable is in describing the "good" events, not how important the variable is likely to be in rejecting "bad" events. If we look at the mean value of chi-squared for hadron events, we find an expression (summing on repeated indices)

$$\zeta = \langle d_i \; H_{ij} \; d_j \rangle = H_{ij} \; \langle d_i \; d_j \rangle =$$
$$= H_{ij} \; D_{ji} = \mathrm{Tr}\,(H\,D)$$
$$\text{where } d_i = X_i \text{ (hadron)} - \langle X_i \text{ (electron)} \rangle$$

If we have now chosen the set of combinations of variables in which H is diagonal (remember H contains only electron information), we find

$$H_{ii} = 1/\sigma_i^2$$
and
$$\zeta = \langle d_i^2 \rangle / \sigma_i^2$$

That is, we have developed the average value of zeta into a sum of terms, giving the mean contribution to chi-squared of each of the variables we have chosen. We now have an ordering criterion on the variables, showing how important each is in generating differences between the pion and electron samples.

3.2 Transition Radiation Detection

Transition radiation detectors (TRD) have been proposed[1,2] as an independent means of discriminating electrons and hadrons from calorimetry. These devices are based upon the detection of few KeV photons radiated by relativistic particles traversing a series of foils of material. Since calorimetric hadron rejection can be expected to work at the level of 1000: 1, it is desired to gain an additional factor of about 100 from TRD in order to reach the overall goal of electron discrimination at 10^5: 1.

Previous studies have shown that a factor of 100 rejection of hadrons can be achieved using several TRD radiator (Li or CH_2) and detector (Xe PWC) packages one after another, together with maximum likelihood analyses based upon total charge collected and cluster counting. The detection of TR photons in the Xe converter zone can be made reasonably efficient; the main background problem comes from the presence of ionization clusters in the gas due to the passage of the charged particles (electrons or hadrons). The primary difficulties for TRD's discussed previously for an SSC[1,2] detector are: (a) The overall depth of proposed detectors (40 - 50 cm) may be uncomfortably large in the constrained world of the 4π detectors; (b) The charge-collection time is rather large (0.5 - 1 μ sec) in comparison with the short mean time between collisions; and (c) the upper limit on momentum for efficient electron discrimination is about 100 GeV/c -- which may be too low for some physics signatures of interest. The work by Y. Ducros reported here is directed at removing these difficulties.

The central idea developed is that transition radiation detection may be incorporated with the general tracking chambers employing short transverse drifts in a Xe-C_2H_6 (50% - 50%) mixture. Arrays of polypropylene foils precede the chambers with spacings chosen to enhance high energy pion rejection.

We have examined the performance of a TRD made of a few radiator-xenon chamber units. The Xe chamber is 4 cm thick and made of hexagonal cells 4 mm diameter with a sense wire at the center. (This structure has been built and tested with a 2 mm cell by R. Bouclier et

al.[16] as shown in Fig. 2.

The chamber is filled with a mixture of Xe -C_2H_6 (50% - 50%), which corresponds to a drift velocity of 45 microns/ns for an electric field between 1300 and 2500 Volts/cm[17]. The time to collect all the charge is 45 ns. This Xe chamber, equipped with 100 MHz FADC or TDC, could be part of the tracking detector. It gives, in addition, a good dE/dx measurement.

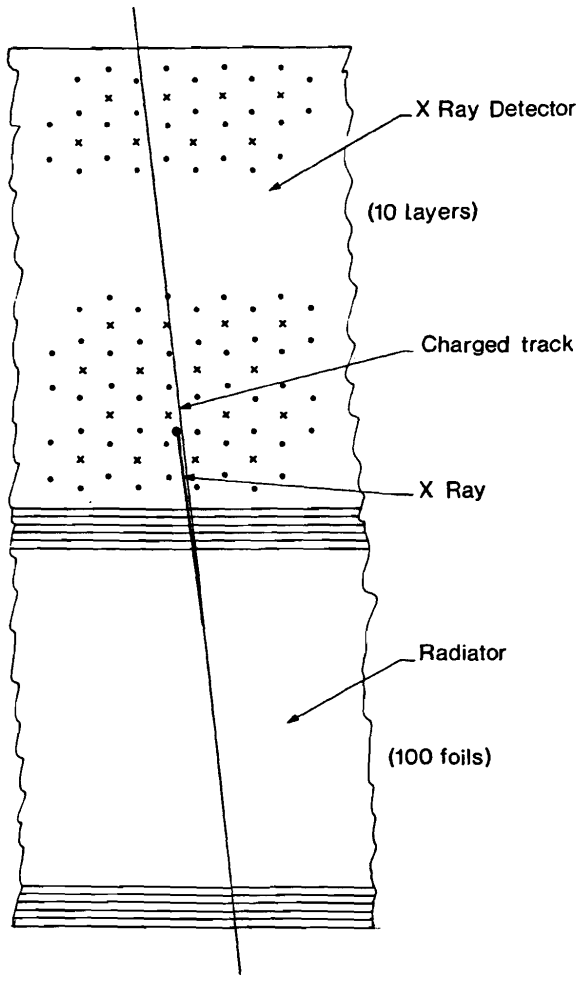

Fig. 2. Schematic diagram of the TRD X-ray detector. Hexagonal cells are made of six potential wires and one sense wire and are 4mm in diameter. The radiator consists of 100 foils of polypropylene 40 microns thick and separated by 900 microns.

The drift direction inside the hexagonal cell is partly along the track and partly perpendicular to the track; therefore it seems difficult to identify individual X-ray clusters. Thus we consider only the total charge collected on each wire.

In order to reduce the sensitivity of detection for ionization charge, we desire a radiator which produces high energy X-rays and apply a cutoff on the collected charge in order to reduce the dE/dx contribution as much as possible. We have considered a radiator made of polypropylene foils 40 microns thick, separated by a gap of 900 microns. These parameters are chosen to increase the energy of the X-rays relative to earlier designs. This optimization raises the pion threshold from 150 GeV/c to approximately 300 GeV/c as shown in Fig. 3. The total thickness of the radiator considered is 10 cm (100 foils). Figure 4 shows the X-ray spectrum detected in the Xe chamber behind the radiator. A cutoff at 8 keV can be applied on the total charge collected in an individual cell. In that case the probability to get more than 8 keV in one cell is 2.1x 10^{-2} for a pion.

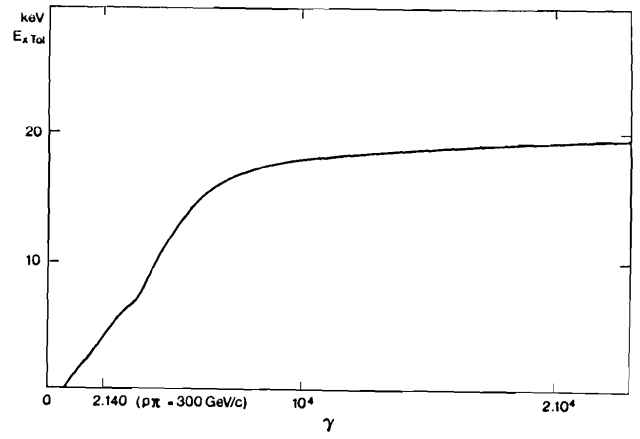

Fig. 3. Total X-ray energy detected in one TRD chamber as a function of The Lorentz factor of the particle.

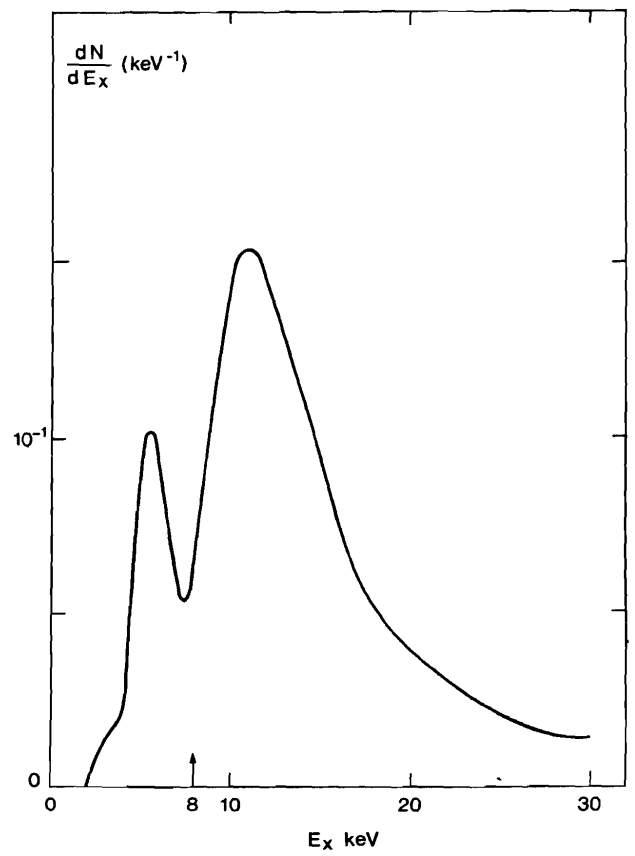

Fig. 4. X-ray spectrum detected in each chamber.

The rejection factor has been calculated in a Monte Carlo program for a set of four radiator/chamber packages, corresponding to a total TRD thickness of 56 cm. We consider only the cells which give more than 8 keV. The electron-pion rejection using the total charge distribution is shown Fig. 5; we find a pion rejection of 34 for an electron efficiency of 90%. Using the number of cells above the threshold the rejection is 220 for the same electron efficiency. Use of refined maximum likelihood analysis techniques could improve the rejection factor. The calculation above has been made for 50 GeV/c electrons and pions. The same calculation for electrons and pions at 300 GeV/c gives a rejection of 5 using total charge and 15 using the number of cells above threshold. All pion rejections computed here are for isolated particles.

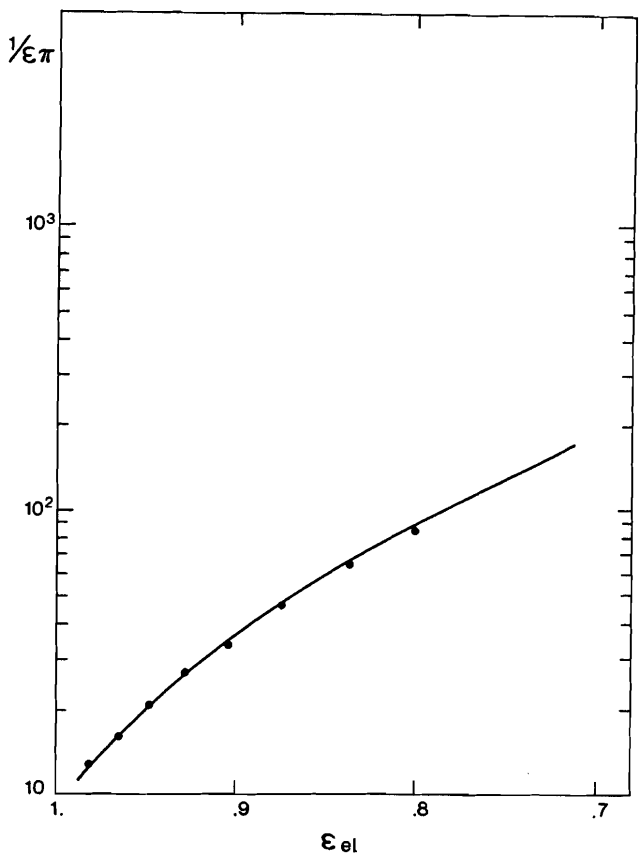

Fig. 5. Pion rejection factor ($1/\varepsilon_\pi$) as a function of electron efficiency (ε_e) using total detected charge in four layers.

The Monte Carlo calculation does not take into account either the variation of the effective thickness of a hexagonal cell as seen by the particles, or the sharing of the cluster charge between two neighbouring cells.

This reoptimization of a TRD for SSC detectors demonstrates that a mixed-function tracking and electron identifying system may be feasible. The charge collection time has been reduced to be roughly commensurate with the bunch crossing time (45 ns vs 16 ns). The operation of a chamber using Xe-C_2H_6 under high rate conditions remains to be established. The reduction in density of the foil packages, made to raise the mean energy of TR X-rays at the expense of TR yield, has the added advantage of reducing the number of radiation lengths in the foils to $.033X_0$ at normal incidence.

3.3 Synchrotron Radiation Detectors

Calorimeters can be used to identify electrons with a rejection against hadrons exceeding 1 part in 1000. For some physics investigations at SSC, rejections of 10^5 are required. The use of transition radiation detectors to achieve an additional rejection power of 50 to 100 for electrons of energies up to 300 GeV is discussed above. Based on the study by J. Butler, we investigate here the possible use of synchrotron radiation to help identify electrons in the energy region above 300 GeV.

Excellent discussions of the physics of synchrotron radiation are given in several SSC publications[1,2,3] so only a summary is provided here. For electrons or positrons of energy E, the energy loss E_L in MeV is given by:

$$E_L[\mathrm{MeV}] = \frac{0.0885\ [E(\mathrm{GeV})]^4\ S}{2\ \pi\ R^2}$$

where R is the radius of curvature of the trajectory and S is the path length traversed in meters. For a particle moving in a plane normal to a field of strength B (kG) and having energy E (GeV), this becomes

$$E_L[\mathrm{MeV}] = 1.26 \times 10^{-5}\ S\ E^2 B^2$$

This frequency spectrum is given by

$$dN_\gamma = \frac{\alpha\gamma S(m)}{2\pi P(\mathrm{GeV}/c)} \times 0.03\ B\ (\mathrm{kG})\ \frac{F(x)dx}{x},$$

with $x = \omega/\omega_c$, the angular frequency of the radiated photons divided by the critical frequency $\omega_c = 3\gamma^3\ c/R$, with c in m/sec and R in meters. The function F(y) is given by

$$F(y) = 2\sqrt{3}\,y \int_{2y}^{\infty} K_{5/3}(x)\ dx,$$

where $K_{5/3}(x)$ is a modified Bessel function of the second kind.

$$N_\gamma = 0.067\ B(\mathrm{KG})S(m) \int_0^{\infty} \frac{F(x)dx}{x}$$

The number of photons is seen to be only a function of B x S which the electron sees and NOT a function of its energy!

The functions F(x)/x and $\int_x^{\infty} F(x)dx/x$ are tabulated in Ref. 1. The result is $N_\gamma \sim 0.57 \times BS$. While N_γ is independent of energy, the frequency spectrum is <u>very</u> sensitive to the energy. Figure 6 shows the evolution of the frequency spectrum as the electron energy is increased from 50 GeV to 1 TeV. The essential point is that at low energies, the electrons emit the radiation in the X-ray region whereas at energies in the hundreds of GeV region they emit gamma rays which not only exceed the pair production threshold but also exceed the "critical" energy for many common materials. (This use of "critical" refers to use energy at which electromagnetic pair production begins to dominate the photon total cross section.)

The final property of synchrotron radiation which must be considered in designing detectors is its angular distribution. The radiation is emitted into a very small angular cone about the particle's instantaneous trajectory. At high energies, it is a good approximation to consider it to be radiated exactly along the tangent. The synchrotron radiation is

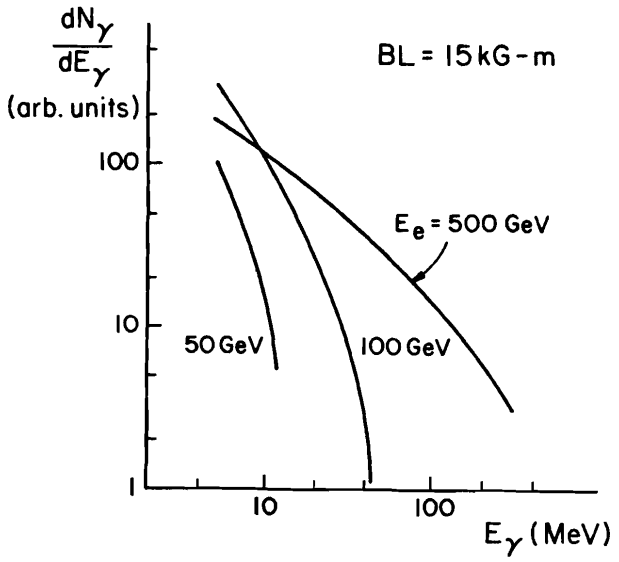

Fig. 6. Distribution of the number of synchrotron radiation photons with photon energy for primary electron energies (E_e) of 50, 100 and 500 GeV. The field integral is 15kG-m.

therefore a fan-shaped object spreading from the tangent to the trajectory at production to the position of the particle itself at the exit to the field region. The separation between the edge of the radiation and the trajectory at the edge of the field volume is

$$d(mm) = \frac{15\ S^2(m)\ B(kg)}{p(GeV/c)}$$

The energy dependence of the frequency spectrum and geometric considerations make the problem of designing detectors fundamentally different at low energies, 5-10 GeV, and high energies, >100 GeV:

a) At low energies, one must detect X-ray photons. One may be able to exploit the characteristic pattern of synchrotron radiation by seeing photons separated from but clearly correlated with, the charged particle trajectories. This technique is employed in the AMY detector at KEK to improve the identification of electrons in the 5-10 GeV region.

b) At high energies, the frequency spectrum shifts so that the photons are above pair threshold. For a field of order 15kG and of size of ~1m, the number of photons of energy >5 MeV is about 10 for electrons of energy >200 GeV. This circumstance is the basis for a detection scheme.

The ability to exploit the "geometric signature" of the radiation will depend on the detector geometry. In the case of a small angle forward detector, we may consider a geometry that has an analysis magnet in the forward direction with an integral BL of approximately 15kG-m or more and a drift space of at least 5 m downstream of the magnet. Under these conditions, the geometric signature might be exploitable up to 1000 GeV. Detection would be accomplished by a gas or liquid calorimeter with a spatial granularity of a few millimeters. Photons would be converted in a set of very thin plates or in the liquid itself. The plates need to be thin to avoid ranging out the electron-positron pairs. This section forms a "natural" good early shower selector which can be useful in the context of the overall calorimetry. Such geometric arrangements have been proposed for SSC detectors.

The integral BL that can be achieved for a central detector is of the order of 15 kG-m so that the frequency spectrum will be similar (at least for normal tracks) to that experienced in the forward geometry. What is lacking is the long drift space which allows the synchrotron radiation to separate from the track and gives an additional geometric handle. Because of this, one is relying solely on the detection of a potentially large number of low energy electrons and positrons early in the EM shower development.

Much has been made in previous studies of the presence of these "highly energetic" synchrotron photons travelling in conjunction with high energy electrons. In order to use their presence to help confirm that a charged particle is an electron rather than hadron, however, it is necessary first to show how to detect the synchrotron photons and then to demonstrate that those hadrons which would have fooled the rest of the electromagnetic calorimetry would "look different" because of the lack of these accompanying synchrotron photons.

The detection of the photons is actually made more difficult by their "high energy". Though they are above pair-production threshold, the pair cross section is only about 1/3 the cross section at asymptotically high energies (thus use of "radiation lengths" is not always appropriate). The electrons, once produced, are in a region where ionization is the dominant energy loss mechanism. Multiple scattering causes the trajectories to be crooked, and there is significant straggling so range-energy relations become complicated.

In the 5-10 MeV region the mass absorption coefficient in lead is about 0.45 cm, with about half the cross section due to the pair production process. Thus with a collection of lead plates of 0.9 cm total, about 3-5 pair conversions will take place and there will be about 6-10 electrons and positrons. These electrons have energies of order a few MeV. To detect them, we must make sure that they don't range out before they reach the sensitive regions of the detector. Using very thin plates of thickness 0.018 cm gives about 0.2 MeV energy loss per foil which, however, increases rapidly as the particle slows down. The foil and sensitive detector arrangement has to be tuned so that a large amount of energy can be absorbed in the sensitive region. The signature for an electron would then be an unusually high pulse height before it initiates the high energy electromagnetic shower. A high energy hadron would exhibit the usual Landau distribution energy loss pattern of a highly relativistic particle. The lack of abnormally high ionization before the beginning of the hadron shower would help tag this as a hadron even if the subsequent shower were "electromagnetic-like". The figure of merit for the separation depends on the average energy deposited in the sensitive early detector by the synchrotron photons compared to the Landau distribution of the highly relativistic hadron. A simple calculation indicates that if the synchrotron radiation can be forced to make a signal greater than 5 times the average pulse height of the hadron, there will be plenty of rejection.

The method outlined for electron/hadron discrimination will work only to the extent that the particles have sufficient path length in the early thin foil portion of the detector so that the synchrotron radiation energy deposit can be seen prior to the main high energy shower development. We note that those

hadrons which are likely to fool the calorimetric shower shape criteria for electrons are those which interact early (and transfer a large fraction of their energy into photons in the first collision via generalized charge exchange reactions). Since we estimate above that the total depth of the synchrotron radiation section is about 1 cm (~2X in lead), there will be a fundamental limit on this method for rejecting hadrons.

The above discussion is obviously qualitative. To determine whether this technique offers real improvement in electron identification, especially in "central" geometries, detailed Monte Carlo studies must be undertaken. They involve the following steps:

1) simulation of the behavior of several 5-10 MeV photons striking the detector.
2) superposition of this behavior on typical electron and positron showers.
3) comparison of the above superposition with the pulse height in the detector of energetic hadrons before they begin to shower.

If these studies indicate some hope for this technique, a prototype detector could be placed in a high-energy beam at Fermilab for further evaluation.

4. Backgrounds for electron identification

The backgrounds present in real detectors arise directly or indirectly from the large flux of hadrons emitted in $\bar{p}p$ collisions relative to the number of electrons. We examine some of these sources here in semi-quantitative fashion, but note the obvious point that proper computation of them can proceed only given a specific detector design. We have also not addressed those backgrounds which may arise from pileup or overlap of tracks from different events.

The three sources of background which can mimic an electron signature are: (1) single pion misidentification, (2) conversion of photons from π°(η, ω etc) decays, and (3) overlaps between a charged hadron and photons within the two particle resolution area.

4.1 Pion misidentification

The ability of calorimeters to distinguish electrons and hadrons has been extensively studied (see Ref. 2, p. 178 for a table summarizing these results). These studies have shown that for high energies (E > 10 GeV), well segmented calorimeters can reject isolated hadrons at the level of 1000 : 1. This rejection has been achieved even when no momentum information is available, using only observed energy deposits and longitudinal and transverse profiles[12]. Use of a measured momentum (comparison of E and p), if applied after all calorimeter cuts, will give a small improvement in rejection below 10 GeV. Use of a veto on energy seen beyond 25 - 30 radiation lengths can improve the rejections at high energy. There is however little prospect for calorimetric rejection of hadrons at significantly higher levels than 1000 since there are physics processes which set a fundamental limit. These come from diffractive analogs of pion charge exchange; e.g.

$$\pi^- p \to A_1^- \; p$$

$$A_1^- \to \rho^- \pi^\circ \to (\bar{\pi} \; \pi^\circ) \; \pi^\circ$$

with the π^- at low energy. Such processes consume an approximately constant fraction of the total interaction cross-section and have been estimated to contribute an electron-like signature at the level of 1 in 3000[18].

Methods for electron identification which are independent of the calorimetry can be used to further enhance pion rejection. Transition radiation detectors are practical for momenta below 300 GeV/c (see section 3.2) and can give uncorrelated rejection factors approaching 100. Above 300 GeV, there is some hope that synchrotron radiation detection could add rejection (section 3.3). Thus for electrons above 10 GeV/c, single pion backgrounds can be suppressed by a factor of 5×10^4 to 10^5. We assume here that electrons (or hadrons) are sufficiently isolated that the showers are distinguishable in the calorimeter.

4.2 Conversion backgrounds

Copious production of π° (and η, ω) in high energy collisions generates a large flux of energetic photons. These photons may convert (internal conversion or external conversion in the unavoidable material in beam tubes, chamber supports etc.) and produce real electron-positron pairs. In such a case, devices which sense the distinction between electron and hadron (calorimeters, TRD etc.) are ineffectual and other measures are sought for background suppression. Control of this background dictates that special care be taken to remove sources of conversion; the ability of a detector to distinguish members of the pair and to flag the absence of a track upstream of material is at a premium. Thus this background source will place particularly strong constraints on the tracking chamber system.

The rejection factor, R, for conversion pair backgrounds can be written

$$R = \left(\frac{dN_D}{dN_P}\right) \cdot P_c \cdot e_{pair} \cdot P_v ,$$

where (dN_D/dN_P) is the parent-daughter relation for pi-zero decay (the ratio of gammas to π° at a given energy); P_c is the total (internal plus external) conversion probability; e_{pair} is the efficiency for detecting the converted pair as two tracks following conversion; and P_v is the probability that a conversion can be vetoed by the absence of a pointing track upstream of the converter.

The parent-daughter factor, (dN_D/dN_P), depends upon the P_T-distribution for the parent π°; for an exponential spectrum, $(dN_D/dN_P) = \langle P_T \rangle / P_T$. However, for the power law spectra observed at large P_T and expected from QCD, the parent-daughter relation approaches an asymptotically constant value. For a spectrum dominated in the large P_T regime by a P_T^{-5} factor, as suggested by QCD, $(dN_D/dN_P) \simeq 0.44$.

The photon conversion probability, P_c, is of course dominated by the material distributed throughout the tracking volume of a detector (Dalitz conversion is equivalent to about $.0077X_o$). A 0.5 mm Be beam tube gives an additional 0.014 X_o at normal incidence. While it is possible to keep the total material traversed in a 4π tracking/TRD detector to $\leq$ 7% X_o at 90°, these conversion material thickness scale like $(\sin\Theta)^{-1}$. Further complicating the problems at small angles, chamber end walls, on-board electronics, cable and gas connections, and the cables themselves add significant material. Even when great care is exercised in minimizing such material, one is likely to have $\lesssim$ 0.2 X_o over the region covered by such end support members ($\Theta \lesssim 15°$). Even after accounting for the relationship

between photon conversion length and radiation length ($L_c = 9\ X_o/7$), one is likely to find that the number of photons is of the order of 1/3 the number of π^o over significant portions of the small angle coverage of a 4π detector. (The parent-daughter relationship discussed above dilutes this fraction since the photons carry lower momentum than their parent meson).

Recognition of a photon conversion can be made in tracking chambers following the converter. Two types of signature can be used: The presence of two tracks emanating from a common origin may be detected or, for overlapped e^+e^- pairs, the doubling of characteristic ionization may be recognized. Seeing two distinct tracks may be aided if a magnetic field is present and the conversion photon is not too energetic. Even without a field, low energy gammas or asymmetric conversions will be visible through multiple Coulomb scattering. Measurement of dE/dx will give good pair rejection for overlapped e ectron pairs so long as additional track overlaps do not occur. With good control of chamber gain systematics and adequate sampling of ionization ($\gtrsim$25), rejection of isolated overlapped pairs at the level of 100 can be achieved.

Details of the pair recognition probability factor, e_{pair}, clearly depend sensitively upon the particular detector configuration. This factor is enhanced in systems with a high density of wire sampling and particular emphasis on dE/dx measurement and on two-track resolution. However, it will generally be true that recognition of pairs will fail when one member of the pair falls below some lower energy limit. This occurs because the low energy electron deviates from the photon direction by a large amount, either through spiralling in a magnetic field or from multiple scattering. One can obtain a crude approximation of the pair conversion detection inefficiency by computing the probability for one electron to have energy below E_{min} (with $E_{min} \sim 100$ MeV in a typical detector). Such a calculation[19] is shown in Fig. 7 for the case of 0.4 X_o with the effects of multiple conversions and radiative effects accounted for). The probability for a photon to produce just one electron above E_{min} is given approximately by $0.9\ (E_{min}/E_\gamma)^{0.9}$.

In this connection, it should be noted that imposing a requirement that just one track emerge from potential conversion material will reduce the efficiency for selecting real electrons. In any finite thickness of material, electrons may radiate photons which then convert and look like pairs. Again imposing a minimum energy cut of 100 MeV after $0.4X_o$ of material, one finds[19] that only 75% of 10 GeV electrons will survive.

The probability to recognize a photon conversion from the absence of a pointing track ahead of the material is also quite dependent on detector detail. In the case of internal conversion or conversion in the beam tube, such recognition is not possible. Even for pair creation in material after some tracking information, accidental overlap of photons and charged tracks can simulate the electron signature. For a cylindrical geometry tracking detector at r=10 cm, $\Theta = 10°$, and $dN_{chg}/d\eta = 50$ (within a jet), the flux of charged tracks is about .015/cm^2. Given realizable two track resolutions, we guess that the pointing track veto factor P_V will not exceed 10-20.

The combined rejection factor against conversions of photons is thus a complex function of detector parameters; it is however seen to increase as angle of production decreases. At 90°, one can likely achieve rejections at or above the 10^5 level possible for charged hadron rejection. At smaller angles, the increase in material thicknesses will enhance the conversion backgrounds so that below some angle, inclusion of explicit electron identifiers (TRD or synchrotron radiation detectors) will be unwarranted. It should be noted however that conversion backgrounds do tend to decrease with increasing P_T (due to the pair recognition veto) so that if large P_T electrons are sought at small angles, TRD's may continue to have some degree of utility.

We stress again that the rejection of conversion backgrounds discussed here requires isolation of photons from other tracks at a level set by calorimeter segmentation and intrinsic shower sizes.

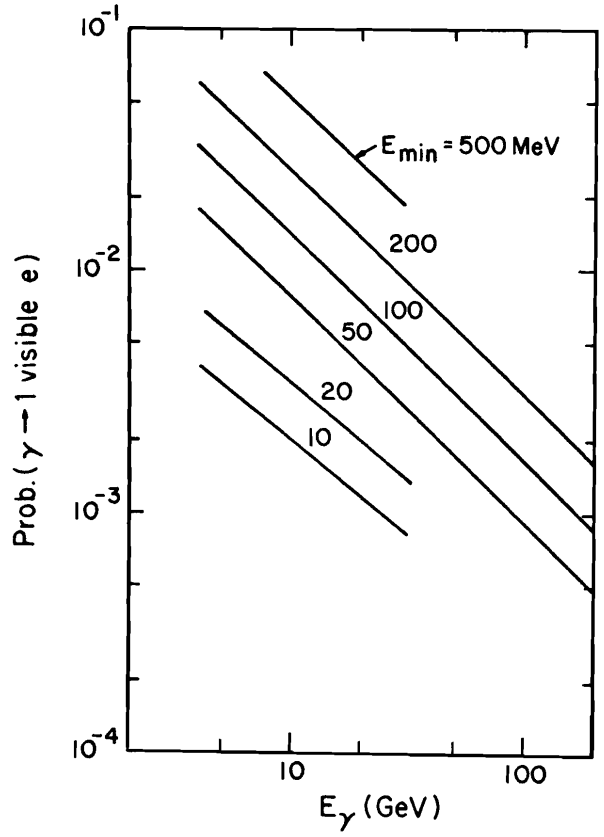

Fig. 7. Probability for a converted photon to yield 1 visible conversion electron vs. photon energy. A visible electron is required to have energy exceeding E_{min}; several values of E_{min} are shown. Photon and electron interactions within $0.4X_o$ Al were used for the calculation.

4.3 Overlap backgrounds

An electron signature can be simulated by the near spatial overlap of a charged hadron and a photon; the hadron supplies the track incident on the calorimeter and photon and hadron together give a shower deposit which may resemble that for an electron. Such an occurrence is obviously most important near the core of jets, where electron identification becomes difficult in any case. There are however a variety of criteria by which an overlap of a single hadron and photon can be discriminated from electrons. Again, detailed calculation of the rejections requires a specific detector geometry as well as a particular physics signature of interest.

A calorimeter, segmented in both depth and transverse coordinates, has itself considerable rejection power for overlaps. One result[12] using an EM calorimeter with fine depth segmentation and one-dimensional transverse segmentation has found that exactly overlapped photons and pions could be rejected at the level of 100 :1. This analysis was performed with the energy spectra appropriate for pions and photons in high energy collisions; it showed that the ratio of energies deposited by photon and hadron in the EM calorimeter was rather uniformly distributed. Thus additional use of a veto on hadron calorimeter energy deposit or comparison of E and p will improve the situation.

Use of specific electron identifiers such as TRD will also aid suppression of the overlap background since the charged track is a hadron. However, the TRD performance is likely to be degraded, relative to that for isolated single hadron backgrounds, since the same physics processes that favor γ-π overlaps also favors production of nearby charged hadrons and such close hadron pairs will be more likely to simulate electron-like TRD response.

The probability for a γ-hadron overlap can be crudely estimated as follows: The particle density in the center of 500 GeV/c jets is approximately[20] 50 charged particles within $\sqrt{(\Delta\eta)^2 + (\Delta\phi)^2} = 0.5$ There are approximately 50 additional photons in this region. For a central calorimeter barrel at r = 250 cm, the area subtended by this jet is approximately 8000 cm^2. An overlap of photon and charged particle must occur within the resolution box set by the ability of the calorimeter to measure shower centroids. Taking this centroid error to be 1 cm (a conservative number for SSC calorimeters), we find the probability for a given charged particle to overlap any photon to be 6×10^{-3}. The probability factor for an overlap signature to simulate an electron, per charged hadron, is approximately $6 \times 10^{-3} \times 10^{-2}$ (calorimeter rejection) $\times 10^{-1}$ (TRD rejection) $= 6 \times 10^{-6}$ This rejection is better than that to be expected for a single hadron misidentification (see section 4.1), so we conclude that the overlap backgrounds will not be dominant in suitably designed detectors, so long as just one photon-hadron pair exist within the transverse cell boundary dictated by calorimeter segmentation.

In the case of each of the backgrounds described, the presence of multiple particles whose showers overlap in the calorimeter will negate the electron identification. Thus detailed statements about the extraction of electron signatures within jets require simulation of specific physics and detector models.

5. Considerations for Detector Design

The desire to obtain good electron identification is one of many constraints imposed upon overall detector design for the SSC. In this section, we examine briefly some of the features which should be considered in optimizing electron recognition. In particular, electron identification places requirements upon calorimeter segmentation (both longitudinal and transverse), tracking chamber wire sampling and charge readout, space available for TRD and/or synchrotron radiation detection, and upon the location of materials for chamber terminations.

5.1 Calorimeter Segmentation

Segmentation of calorimeter readout for 4π detectors is dictated by many, often conflicting, demands:

1) Control of charged particle-photon overlap backgrounds for electrons.
2) Ability to isolate electrons or muons from nearby particles.
3) Single hadron rejection.
4) Accuracy of P_T measurement.
5) Topological identification (e.g. high mass WW pairs vs QCD jets).
6) τ identification.
7) Space requirements for connections, preamplifiers etc..
8) Signal collection logistics.
9) Noise contributions.
10) Cost.

It is commonly argued that since transverse EM sizes are small ($\lesssim$ 1 cm), the EM calorimeter should ideally have transverse segmentation at about this level (corresponding to $\Delta\eta = \Delta\phi \leq 0.01$ or 2 cm x 2 cm towers for calorimeters located at about 2 m from the interaction point). A more relaxed requirement can be inferred from studies of the WW pair identification problem[13,21] (point 4 above). These studies indicate that $\Delta\eta=\Delta\phi=0.03$ may be sufficient. Requirements on shower centroid measurement (point 1) for controlling overlap backgrounds suggest that transverse sizes of towers ought not exceed about 5 cm. Our qualitative interpretation of these statements is that transverse segmentation of calorimetry in the range $\Delta\eta = \Delta\phi = (0.02 - 0.03)$ should be adequate for much of the solid angle. For an effective radius of EM calorimetry of 250 cm, this implies tower sizes of 5-10 cm. Although this is larger than EM showers, we note that the scale of hadron showers is in fact 10-30 cm and that segmentation very much finer than this is not warranted in view of the desire to select isolated electrons (point 2).

The longitudinal depth of the EM calorimeter should be set so that at least 95% of the EM energy is absorbed. The remaining energy can be seen in the first portion of the hadron calorimeter, or inferred from the observed longitudinal profile in the EM section. A depth of 25 X_0 seems adequate.

The longitudinal segmentation is important for rejecting hadron induced backgrounds to electrons. One study[12] showed the electron identification suffers markedly when there are fewer than three depth segments and that four is better than three. One of these segments should be located near the expected EM shower maximum (5-12 X_0).

In order to better determine photon and electron directions, it is often advocated that some fine segmentation layer be inserted in the EM calorimeter, presumably near shower maximum. The question arises whether this finer readout should take the form of strips which have excellent resolution in one dimension, or of further subdivision of the normal square pad towers. Studies of 2 TeV detector calorimeters[22,23] have shown that relatively little advantage is gained in shower centroid location using strips. Moreover, the fact that long strips sample spatial regions of an event which are quite different from those of the towers implies that disentangling the ambiguities due to multiple hits in a high multiplicity event would be

quite difficult. If subdivision of a segment of the EM calorimeter is desirable, we strongly favor simple partitioning of the basic tower structure.

A segmentation scheme for the central region of the EM calorimetry in a 4π detector is outlined below[24]. We have imposed the arbitrary constraint that the number of readout signals (Θ>10°; $\eta \leq 2.5$) be limited to $\leq 3 \times 10^5$. For definiteness we take the effective calorimeter surface to be a cylinder of radius 250 cm for $\eta \leq 1$ and a plane perpendicular to the beam at z = 300 cm for $1.0 \leq \eta \leq 2.5$.

The barrel region segmentation is $\Delta\eta$=0.02, $\Delta\phi=2\pi/300$ for a total of 30,000 towers. The size (Δz) of a cell varies from 5 cm at 90° to 7.8 cm at 45°. In the forward region, we set $\Delta\eta$=0.02 at the outer radius, becoming $\Delta\eta$=0.056 at the inner radius ($3.0 \leq \Delta r \leq 6.6$ cm) for a total of 40 rings. Phi subdivision is $\Delta\phi=2\pi/300$ in the outer 20 rings and $2\pi/150$ for the inner 20 rings. The two end calorimeters together contribute 18,000 towers.

All regions are divided into three longitudinal sections ($4X_0$, $7X_0$, $14X_0$) with the middle section subdivided into one half the normal $\Delta\eta$, $\Delta\phi$ dimensions. Thus the largest small pad size is 3.9 x 2.6 cm^2 which should be adequate for shower localization. The total number of signals is 288K.

We note in passing that, the presence of a magnet coil ($\sim$ 1.3 X_0) before the calorimeter should have little effect on energy resolution or upon electron identification - providing that some attention be given to sampling the energy deposited in the first section following the coil. This could be a "massless gap" at the beginning of the calorimeter. It is possible that the first readout section could accomplish this purpose, but this point requires some further study.

5.2 Tracking constraints

The requirements imposed by the tracking and momentum measurement needs are often different from those imposed by the desire to identify electrons with transition radiation detectors[25]. In the tracking chambers, a premium is placed on excellent time measurement for best momentum resolution; suppression of electron pair backgrounds and detection of transition radiation X-rays requires good charge measurements. Pattern recognition of track segments suggests that the track chambers occupy clustered regions of space rather than being homogeneously distributed. Use of small cells and fast gas in tracking chambers is dictated by the short inter-bunch timing, whereas TRD chambers must employ a gas rich in a high Z component (Xe).

Although we raised the possibility of a combined TRD/tracking system in section 3.2, using 4 mm cells, Xe-C_2H_6 gas and a flash ADC readout, the above constraints may argue for a design which separates tracking and TRD. This is enabled by the layout of the 4π detector tracking system in which gaps are introduced between supercells of the chambers[25,26]. A possible layout of the tracking/TRD volume is shown in Fig. 8. The central region includes four foil/chamber TRD packages lumped in the regions $70.5 \leq r \leq 103.5$ cm and $164 \leq r \leq 197$ cm. Each package is 15 cm deep and has a Xe-ethane readout chamber with 8 sense wire layers and a 4 mm transverse spacing. The central TRD wire count is approximately 65,000.

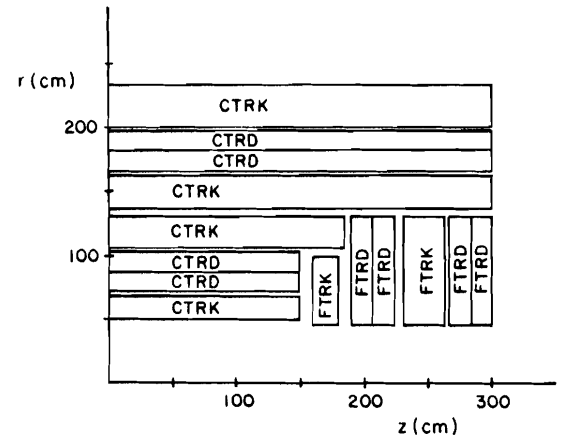

Fig. 8. Schematic layout of one quadrant of tracking chambers (CTRK and FTRK) and transition radiation detectors (CTRD and FTRD). C and F denote central and forward respectively.

Forward TRD packages of similar granularity are shown, again in two distinct regions between tracking sections. These will bring the total TRD signal count to about 10^5. Each signal channel requires waveform digitization electronics in order to measure both charge deposit and time. With a drift speed of 4.5 microns/ns these chambers integrate over 2-3 bunch crossings. We expect spatial resolution in the TRD chambers of about 200 microns.

The spatial arrangement of tracking and TRD is made to give full coverage for electrons in the central TRD's out to η = 1.2. Between η = 1.2 and η = 1.3, the coverage by TRD is impaired (2 of 4 packages). From η = 1.7 to the inner edge at η=2.4, full TRD coverage is regained. The location of chamber ends is concentrated in the region $1.25 \leq \eta \leq 1.5$; this angular zone will suffer from large pair conversion backgrounds, so that the absence of full TRD rejection there is not of great importance. The minimum angle subtended by tracking and TRD is about 10°; inside this angle, the track density grows substantially and we assume that special chambers at large z will be employed. TRD coverage inside 10° is probably unwarranted since the maximum momentum for pion rejection (300 GeV/c) implies an upper limit on P_T of 50 GeV/c. In fact, as discussed in section 4.2, the entire question of the utility of the forward TRD system rests on the ability of the tracking system to suppress pair conversion backgrounds.

5.3 Forward detectors

The region inside Θ=10° is likely to be covered by somewhat special detectors extending many meters downstream of the interaction point. If electron identification is required, special consideration is required owing to the large momentum of the small angle particles. Use of synchrotron radiation detectors based upon separation of track ionization and synchrotron photons is an attractive possibility. As discussed in section 3.3, one needs a magnetic field region of 15 kG-m followed by a 5 m drift space for photon-track separation. Detection of the few MeV photons can then be accomplished in a chamber comprising a few radiation lengths and good spatial resolution in the bend plane.

REFERENCES

We abbreviate references to articles in Proceedings of The Summer Study on The Design and Utilization of The Superconducting Super Collider, ed. R. Donaldson and J. Morfin, Snowmass CO (1984) by "Snowmass 1984".

1. G.B. Yodh et. al., "Electron Identification" in Snowmass 1984, p. 523.
2. Report of The Task Force on Detector Research and Development for the Superconducting Super Collider, M. Gilchriese et. al. SSC-SR-1021 (June 1986) (p. 176).
3. S. Aronson, Proceedings of The 1983 DPF Workshop, Berkeley CA (1983).
4. Physics at the Superconducting Super Collider, ed. B. Winstein, Fermilab (1984).
5. J. Carr and E. Eichten, Snowmass 1984, p. 703.
6. J. Gunion et. al. report on Higgs Particle signatures, these proceedings.
7. B. Cox and F. Gilman, These proceedings.
8. K. Lane and J. Rohlf, Snowmass 1984, p. 737.
9. S. Dawson and A. Savoy-Navarro, Snowmass 1984, p. 263.
10. D. Wagoner and B. Cox, These proceedings.
11. Y. Fukui et. al., "e/π Separation in The CDF End Plug EM and Hadron Calorimeters", These proceedings.
12. R. Engelmann et. al., Nucl. Instr. and Methods 216 (1983), 45.
13. J.M. Hauptman, Snowmass 1984, p. 121.
14. Report of The W-Pair Identification group, these proceedings.
15. H. Wind, Formulae and Methods in Data Evaluation, vol 3, section K (European Physical Society, 1984).
16. R. Bouclier et. al., CERN preprint EP/85-169.
17. A. Peisert and F. Sauli, CERN preprint EP/84-08.
18. M.L. Good, private communication.
19. C. Klopfenstein and M. Strovink, D0 internal note 250.
20. F. Paige, private communication.
21. E. Fernandez et. al., Snowmass 1984, p. 107.
22. S. Stampke, D0 internal note 396.
23. M.L. Stevenson, D0 internal note 359.
24. See The Reports of The Calorimeter group and The Calorimeter Segmentation group in These proceedings for further discussion of segmentation schemes for SSC detectors.
25. Report of The Tracking group, These proceedings.
26. Report of the 4π Detector group, These proceedings.